Journal of Non-Newtonian Fluid Mechanics 210 (2014) 1–11

Contents lists available at ScienceDirect

Journal of Non-Newtonian Fluid Mechanics

journal homepage: http://www.elsevier.com/locate/jnnfm

Prediction of excess pressure drop in contraction–expansion flow by molecular dynamics: Axisymmetric and planar configurations

J. Castillo-Tejas [a,*], O. Castrejón-González [b], J.F.J. Alvarado [b], O. Manero [c]

[a] Facultad de Ciencias Básicas, Ingeniería y Tecnología, Universidad Autónoma de Tlaxcala, Calzada Apizaquito S/N, Apizaco, Tlaxcala 90300, Mexico
[b] Departamento de Ingeniería Química, Instituto Tecnológico de Celaya, Avenida Tecnológico y García Cubas S/N, Celaya, Guanajuato 38010, Mexico
[c] Instituto de Investigaciones en Materiales, Universidad Nacional Autónoma de México, Ciudad Universitaria, México, DF 04510, Mexico

ARTICLE INFO

Article history:
Received 4 December 2013
Received in revised form 30 April 2014
Accepted 5 May 2014
Available online 15 May 2014

Keywords:
Non-equilibrium molecular-dynamics
Excess pressure drop
Contraction–expansion flow

ABSTRACT

In this paper, non-equilibrium molecular dynamics is used to simulate the flow of a dilute solution of linear molecules (Boger fluid) and a simple fluid (Lennard-Jones) through axisymmetric and planar contraction–expansion geometries. The pressure flow condition is generated by adding an external force field F_e to the equation of motion for the velocity, which is coupled to Nose–Hoover dynamics to keep the temperature constant. According to the monomer-spring model of Kremer and Grest, linear molecules are represented; and the simple fluid consists of spherical particles, which interact by means of a Lennard-Jones potential. The rheological response of the fluids indicates that the Boger fluid and the simple fluid exhibit constant viscosity in the interval ($0.002 \leqslant \dot{\gamma} \leqslant 0.5$); additionally, the Boger fluid presents elastic effects under shear (first normal stress difference, N_1) which are quadratic at low shear rates. In pressure flow through the expansion–contraction, results indicate that when both fluids have the same viscosity, pressure profiles $P(x_1)$ in the axisymmetric geometry reveal a higher pressure drop (ΔP) in the Boger fluid, while in the planar geometry ΔP was the same for both fluids. Results also reveal that ΔP is closely related to the extensional strain rate ($\dot{\varepsilon}$) experienced by the fluid at the contraction entrance. The pressure drop is higher in the axisymmetric geometry because the change in the molecular conformation, as measured by the mean-square mass distribution tensor $\langle I_2^2 \rangle$, is 80% higher than in the planar case, resulting in an increase in the energy required to deform the molecule and the loss of mechanical energy. In the planar geometry, under the same extensional strain rate, the conformational change of the molecules in the Boger fluid at the contraction is then lower than in the axisymmetric geometry.

1. Introduction

This research work examines one of the benchmark problems in rheology, namely, the prediction of the excess pressure drop in the flow of non-Newtonian fluids through contraction–expansion geometries. Experimental studies show that polymer solutions of the Boger type exhibit a larger pressure drop than its Newtonian counterpart, both of the same viscosity, in axisymmetric but not in planar geometries. As discussed below, experimental evidence on the flow in micro-devices contraction–expansion suggests that at very high strain rates that are achieved in these devices, such excess pressure drop could also be observed in a planar configuration.

Nigen and Walters [1] performed experiments to reproduce the flow of two polymer solutions of constant viscosity, Boger fluid type, through axisymmetric and planar contractions; experiments were also replicated using Newtonian fluids with the same viscosity of the Boger fluid. In the axisymmetric configuration, results indicated that the Boger fluid exhibits larger pressure loss than the Newtonian fluid, and that this loss depends on the viscosity of the fluid and the vortex formation at the input of the contraction. Surprisingly, in the planar configuration, the Boger fluid exhibited the same pressure loss as the Newtonian liquid with absence of vortices at the input of the contraction. It is noteworthy that the experiments developed by Nigen and Walters [1] considered a wide range of contraction ratios ($2 \leqslant \hat{\beta} \leqslant 40$) and to achieve planar flow conditions in the rectangular configuration, the length of the contraction in the neutral direction L_3 was considerably larger than that in the flow direction L_1 and that of the gradient L_2. Finally, the authors conclude that the extensional strain rate is similar both in planar and in the axisymmetric configuration. A further study [2] confirms the relationship between the formation of vortices and excess pressure drop. In a work parallel to that of

* Corresponding author. Tel.: +52 241 41 72544; fax: +52 241 41 75844.
E-mail address: j_castillo_tejas@hotmail.com (J. Castillo-Tejas).

http://dx.doi.org/10.1016/j.jnnfm.2014.05.001
0377-0257/

Nigen and Walters [1], Rothstein and McKinley [3] performed experiments to reproduce the flow of a solution of polystyrene Boger type through an axisymmetric expansion–contraction, with a contraction ratio of 4:1:4, where the Boger fluid and Newtonian viscosities were similar. Their results indicate the existence of an extra pressure drop in the Boger fluid above the one observed in the Newtonian liquid at the same flow rate, which increases monotonically with the Deborah number. They state that this extra pressure drop is associated with cycles of stress-conformation hysteresis and dissipation processes, such that the stress and end-to-end distance of the polymer molecules follow a path at the contraction entrance and they return to equilibrium through a different trajectory.

Apparently, the occurrence of hysteresis cycles and their relationship with viscous dissipation, as well as the extensional strain rate experienced by the fluid entering through the contraction are related to the existence of *epd* (excess pressure drop) in axisymmetric configurations. The existence of these hysteresis cycles has been experimentally and numerically predicted (at different length scales) [4–7]. Using non-equilibrium molecular dynamics, it has been established that in the flow of polymer solutions through the contraction–expansion geometries, the largest pressure loss occurs at the entrance of the contraction, and in this area of the flow domain a maximum in the viscous dissipation and extensional strain rate are revealed [7].

Apparently, the absence of the excess pressure drop in planar configurations is due to the low elastic response that the fluid exhibits in this geometry [2]. In this regard, it has been found that the extensional strain rate ($\dot{\varepsilon}$) experienced by the fluid depends on the geometry and contraction ratio ($\hat{\beta}$). In the axisymmetric geometry the extensional strain rate scales with the square of the contraction ratio ($\dot{\varepsilon} \approx \hat{\beta}^2$) while in the planar case the variation is linear ($\dot{\varepsilon} \approx \hat{\beta}$) [8–10]. Genieser et al. [11] states that the planar extensional flow through a slot induces a non-linear viscoelastic response of the fluid, and that this response cannot be substantially modified by changing the contraction ratio ($\hat{\beta}$). Recently, Castillo-Tejas et al. [7] simulated the flow of a solution of linear molecules and that of a single fluid, Lennard-Jones type, through an expansion–contraction planar configuration 2:1:2, using the molecular dynamics technique. The density of both fluids was chosen such that the fluids exhibit the same shear viscosity in the first Newtonian region of the flow curve (η versus $\dot{\gamma}$). It was found that the ratio Lc_1/Lc_2 (the length of the contraction in the flow direction (x_1) and in the gradient direction (x_2), respectively) affects substantially the pressure drop. When the ratio Lc_1/Lc_2 is equal to one, both fluids exhibit the same pressure drop, viscous dissipation and extensional strain rate; however, by increasing the ratio Lc_1/Lc_2 in the Boger fluid, larger pressure drops are predicted than those of the simple fluid (or Lennard-Jones fluid) with $Lc_1/Lc_2 = 1.0$. With values of the ratio Lc_1/Lc_2 larger than one, the Boger fluids experiences higher extensional strain rate and larger area of stress-conformation hysteresis. The strain rate ($\dot{\varepsilon}$) and hence the extensional stress are related to conformational changes of the fluid molecules through the contraction, and therefore, the molecular conformation along the flow path is different in axisymmetric and planar geometries.

The number of works using micro-devices to characterize and study the response of polymer solutions in extensional flow has increased. Recently, cross-slot micro-devices have been used to reproduce the extensional flow of diluted and semi-diluted solutions, obtaining information on stagnation points from measurements of pressure drop and birefringence [12–15]. Rodd et al. [16] used a 16:1 planar micro-contraction to study the flow field and the pressure drop of a polyethylene oxide solution, and found that there are significant extensional effects due to the very small length scales and to the associated high extensional strain. Additionally, the authors identified four flow regimes in the pressure drop measurements; elsewhere, similar conclusions were obtained [17,10,18–20].

Large extensional strain rates reached in micro-devices may enable elastic fluids to generate larger pressure drops than their Newtonian counterpart in planar geometries. Campo-Deaño et al. [21] reproduced the flow of a low viscosity Boger fluid through a planar hyperbolic micro-contraction (the fluids were prepared with aqueous polyacrylamide solutions of different concentrations to which sodium chloride is added). The rheological response of the solutions indicated that the addition of salt to the solution produces a viscosity decrease, such that at low concentrations the fluid exhibits a constant viscosity range similar to that of a Boger fluid. Results indicate that the pressure drop is larger in the Boger fluid than in the Newtonian liquid (water). However, it is important to note that the Boger fluid viscosity (aqueous solution of polyacrylamide) was larger than that of the Newtonian fluid (water), and that this difference in viscosity may be responsible for the larger pressure drop in the Boger fluid. The same issue should be considered in the pressure drop results of planar micro-contractions [16,22], and in previous works with molecular dynamics [6]. It is important to note that the *epd* reported by Nigen and Walters [1], and Rothstein and McKinley [3,8] in axisymmetric configurations considered that the viscosity of Boger fluid is similar to that of its Newtonian counterpart. In the present paper, predictions of the excess pressure drop are made taking care that the viscosity of the fluids in question is the same.

Presently, there are numerous numerical simulations at the continuum mechanics level oriented to predict the *epd*, as well as the number of constitutive equations used to reproduce the kinematics and dynamics of flow see [23–28]. In most works, shear thinning polymer solutions or Boger fluids are used, where predictions of the pressure drop are below the value exhibited by the Newtonian fluid (i.e., $epd < 1$). For example, Szabo et al. [23] use a FENE-CR model to simulate the flow of a Boger fluid through a 4:1:4 axisymmetric contraction–expansion. Their results indicate that at low Deborah numbers, the *epd* is less than one and depends on the extensibility parameter of the model (maximum extension of the polymer molecules). There are recent works [29,30] which state that the failure of the Oldroyd-B model in predicting the *epd* is associated with a strong dependence of the first normal stress difference N_1 respect to shear rate $\dot{\gamma}$ (quadratic for all shear rates). For axisymmetric configurations, it is shown that the prediction of *epd* depends on a balance between extensional viscosity η_E and N_1. The results are consistent with previous works establishing the importance of extensional stress in the flow through contraction geometries [31–34].

A review of experimental works and numerical studies reach the following conclusions: (1) when the viscosity of Newtonian and non-Newtonian fluid is similar, *epd* has been observed in axisymmetric but not in planar macro geometries; (2) *epd* is apparently related to the formation of vortices at the entrance of the contraction, hysteresis cycles, viscous dissipation and extensional strain rate; (3) the use of constitutive equations and continuous models has been partially successful in predicting the *epd*, and the success depends on a balance between the extensional viscosity (η_E) and the first normal stress difference (N_1); (4) and finally, an important issue is the extensional strain rate experienced by the fluid which again depends on the particular geometry. Based on the above conclusions, the objective of this work is to simulate the flow of two liquids (one Newtonian as a Lennard-Jones Fluid and a Boger fluid) of the same viscosity through contraction–expansion geometries both axisymmetric and planar. Simulations calculate the pressure field, velocity and molecular conformation along the central line of confinement. The analysis of these predictions aim to reveal important features on the origin of the *epd*.

The manuscript is organized as follows. Section 2 presents the simulation method. Sections 3 and 4 deal with the construction of the simulation region and calculation of the rheological properties. Section 5 includes the rheological response of fluids under simple shear flow. Section 6 analyzes the effect of molecular structure on the extensional rheology and excess pressure drop in planar and axisymmetric geometries. Finally, in Section 7 a discussion and the main conclusions are presented.

2. Theory and simulation method

2.1. Units system

In real units, the molecular dynamics technique involves the use of length and time scales of the order of 10^{-9} m and 10^{-12} s, respectively, such that carrying out simulations with these numerical values can lead to overflow or underflow problems as a result of floating point operations. Therefore, it is a common practice to simulate the flow using reduced (or dimensionless) units. In this paper we use the Lennard-Jones potential to reproduce a portion of the interactions between components of fluid under consideration, such that their energy parameter (ε) and length (σ), together with the mass of the particle (m_i) are selected to reduce all variables associated with the simulation. Table 1 shows the relationship between the parameters ε, σ and m_i used to express, in dimensionless form, the relevant variables.

2.2. Systems under study

Fluids considered (see Fig. 1) include a solution of linear molecules, a Boger fluid ($\rho = 0.84$) and a simple fluid or L-J Fluid ($\rho = 0.87$) constituted by spherical particles; both fluids at a reduced temperature of 3.0. As shown in Fig. 1, the Boger fluid includes M linear molecules, each one with twenty linked sites, immersed in S spherical particles (the solvent). The simple fluid is made of S spherical particles. Based on Fig. 1, the molecules of the Boger fluid are represented according to the monomer-spring model of Kremer and Grest [35]. This model considers that the molecular chain is represented by a spring and the mass is concentrated in a monomer or site. A molecule as a collection of sites connected through non-harmonic springs is then envisaged. In Table 2, the total number of sites (N) used in the simulations is included, for both fluids and flow configurations. In the planar configuration, N is equal to 15,000 sites that in the case of the solution, involves 75 (M) molecules and 13,500 (S) solvent particles. In axisymmetric configurations, N is fixed depending on contraction ratio, for example, the solution consists of 362 molecules and 65,060 solvent particles at a $\tilde{\beta} = 4$.

In molecular dynamics formulations, the motion of particles in the system is described by classical mechanics including particle-particle interactions. The detailed interaction among particles is given by summation of the overall pair-pair contributions according to $U(\mathbf{r}^N) = \sum_i \sum_{j>i} U(r_{ij})$, where $U(\mathbf{r}^N)$ is the potential energy of the configuration, $U(r_{ij})$ is the energy between pairs of particles, and r_{ij} is the scalar distance between i and j particles, respectively.

The functional form of the intermolecular potential for these fluids has already been detailed in a previous work [7] and involves the use of non-linear finite-extensible elastic potential (FENE) [36] and the Lennard-Jones potential, the latter truncated and shifted at a cutting distance $r_c = 2^{1/6}\sigma$.

Table 1
Some quantities expressed in Lennard-Jones reduced units.

Physical quantity	LJ unit
Length	σ
Mass	m
Energy	ε
Number density	$1/\sigma^3$
Temperature	ε/k_B
Time	$(m\sigma^2/\varepsilon)^{1/2}$
Volume flow rate	$(\varepsilon\sigma^4/m)^{1/2}$
Stress	ε/σ^3
Viscosity	$(m\varepsilon)^{1/2}/\sigma^2$
Shear rate	$(\varepsilon/m\sigma^2)^{1/2}$

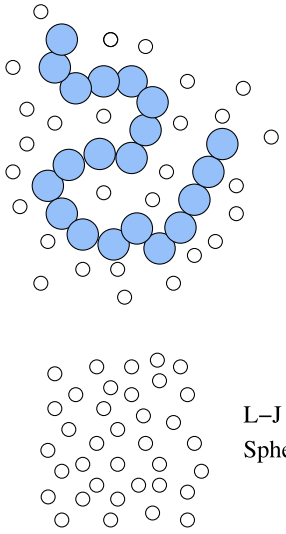

Fig. 1. Schematic representation of fluids under study.

Table 2
Information on number of sites per system and configuration; and dimensionless lengths of the simulation regions.

	Axisymmetric		Planar
	2:1:2	4:1:4	2:1:2
Particles in the system			
L-J Fluid			
S	75,440	74,120	15,000
Solution of linear molecules			
M	368	362	75
S	66,240	65,060	13,500
Dimensions of each region			
L_1	163.24	163.24	192.92
Lc_1	14.84	14.84	14.84
L_2	–	–	29.69
Lc_2	–	–	14.84
L_3	–	–	3.22
			3.12 (L-J)
D_1	14.28	7.14	–
D_2	28.56	28.56	–

2.3. Equations of motion

A Poiseuille flow is generated through an axisymmetric (or cylindrical) and rectangular (or planar) contraction–expansion geometry. The essence of molecular dynamics is the motion estimation of a set of particles that obey the laws of classical mechanics by solving the equations of motion. In the case of Poiseuille flow, the equations used include an additional term (external field of force F_e) to produce the flow [37,38] and are given by:

$$\frac{d\mathbf{r}_i}{dt} = \mathbf{v}_i \tag{1}$$

$$\frac{d\mathbf{v}_i}{dt} = \frac{\mathbf{F_i}}{m_i} + \frac{F_e}{m_i}\mathbf{e}_1 - V_\xi \mathbf{v}_i \tag{2}$$

$$\frac{dV_{\xi}}{dt} = \frac{1}{Q}\left[\sum_{i=1}^{N} m_i v_i^2 - \frac{L_s}{\beta}\right] \tag{3}$$

where m_i and $\mathbf{F}_i$ are mass and force associated with particle i, whereas the force on particle i is the result of its interaction with other system components, $\mathbf{r}_i$ is the position vector of particle i and $\mathbf{v}_i$ represents its velocity with respect to the laboratory frame of reference (i.e., the sum of the peculiar and streaming components). The peculiar velocity is the rate of change of the position of the particle under equilibrium conditions, i.e., in absence of external perturbations. The fluid motion is generated by an external force field F_e in Eq. (2), where the unit vector $\mathbf{e}_1$ indicates the direction (x_1) in which F_e is applied, such that, $F_e = 0$ for v_2 and v_3 components of Eq. (2). It is noteworthy that F_e is only applied to the input of the simulation region. Viscous heating is generated by fluid motion, which needs to be removed from the system to keep the temperature constant, and in so doing, the Nose–Hoover thermostat [39] is coupled to the equations of motion. As shown in Eq. (2), the thermostat controls the temperature of the system by scaling the velocity of each particle with a dynamic variable – V_{ξ}. The thermostat is only applied to the v_2 and v_3 components of Eq. (2), and as a result the fluid develops a streaming velocity in the x_1-direction and a peculiar velocity along the x_2 and x_3 directions. In all the simulation work, it is verified that v_1 is a streaming velocity, and v_2 and v_3 are peculiar velocities. This consideration modifies the calculation of the degrees of freedom of the thermostat (L_s) and the term $sum_{i=1}^{N} m_i v_i^2$ in Eq. (3). Finally, in Eq. (3), Q is the associated mass of thermostat and β is the reciprocal of the reduced temperature.

Although v_2 and v_3 components of velocity vector are peculiar velocities, the flow dynamics is consistent with local secondary flows that are observed in contraction–expansion geometries. In these geometries a two-directional flow exists just before the fluid enters the contraction, such that, $v_1 = v_1(x_1, x_2) \neq 0$ and $v_2 = v_2(x_1, x_2) \neq 0$ and additionally, vortex formation at the contraction exit is present. The predictions of vortex formation [6] and a two-directional flow at the contraction entrance [40] implies a momentum flux of near zero in these regions of geometry, which is consistent with the definition of peculiar velocity. In molecular dynamics simulations of the flow through contraction–expansion geometries [6,7], it has been shown that the rate of energy removed by thermostat is equivalent, as a first approximation, to the rate of energy dissipation. Such equivalence allows justifying the application of the thermostat in a consistent manner with flow dynamics.

3. Geometry and simulation method

Fig. 2 presents the simulation region for the two geometries, and in both the solution of the equations of motion is performed considering a Cartesian coordinate system, with origin at the center of contraction. It is noteworthy that with the forces and position coordinates in x_2 and x_3 directions of each particle, its radial and angular coordinate in cylindrical region are obtained as well as the force in the radial direction. As shown in Fig. 2, in the cylindrical region there is a total confinement in the radial direction, so that periodic boundary conditions and minimum image condition are applied in the flow direction. With regard to the confinement, in previous studies of molecular dynamics [6,40,7] stochastic walls have been used to simulate flow of complex fluids through contraction–expansion in a planar configuration. However, this methodology was not implemented in both geometries used in this work, and a repulsive potential instead is used to describe the surface and prevent the particles to cross the walls.

With respect to the rectangular geometry, the confinement is normal to the direction of the gradient x_2, and the periodic boundary conditions and minimum image criteria are applied in the flow direction x_1 and neutral direction x_3. Table 2 lists the dimensions of simulation regions expressed in dimensionless units, estimated from the definition of reduced density per site and the number of molecules for each system. In both geometries the contraction ratio was fixed to $\hat{\beta} = 2$, and in the case of the axisymmetric geometry, $\hat{\beta} = 4$ was also included. For the cylindrical geometry, the dimensions of the simulation region are the same for the Boger and LJ fluids; therefore, the total number of particles is set according to the fluid density. In the rectangular geometry the particle number is set to 15,000, such that taking into account the dimensions of the region of simulation in directions x_1 and x_2, and the density of each fluid, the length of the simulation region in neutral direction (x_3) can be calculated.

In a recent work [7] it has been shown that the ratio Lc_1/Lc_2 or Lc_1/D_1 in the planar and cylindrical geometries, respectively, are important parameters in predicting the rheological response of the fluids through the contraction. For the cylindrical geometry, Lc_1/D_1 has a value of 1.04 and 2.08 for $\hat{\beta}$ equal to 2 and 4, respectively. For the 2:1:2 rectangular geometry, Lc_1/Lc_2 is maintained at a value of 1.0.

The non-equilibrium simulations carried out to reproduce the flow condition require an initial configuration, which it is obtained from equilibrium molecular dynamics. The generation of this initial configuration was different for each type of geometry. For the rectangular region, the position vectors $\mathbf{r}_i^N$ ($t = 0$) for the 15,000 sites are located on a lattice in the whole simulation domain, which, in addition to the velocity vector $\mathbf{v}_i^N$ ($t = 0$) and force $\mathbf{F}_i^N$ ($t = 0$), are used as an initial condition to obtain the dynamics of the system in the absence of external perturbations. However, in the cylindrical geometry it was not possible to equilibrate the systems (mainly because of bond ruptures near the contraction) when the vectors $\mathbf{r}_i^N$ ($t = 0$) were assigned in the whole simulation domain. A strategy was developed performing equilibrium molecular dynamics simulations in cylindrical channels with the same dimensions of the contraction and expansion. For example, to obtain the initial configuration of the molecules solution in the cylindrical geometry with $\hat{\beta} = 2$, initially two configurations were generated in cylinders with dimensions of length and diameter of 14.84σ by 14.84σ, and 74.2σ by 28.56σ, respectively. The resulting configurations are subsequently coupled with equilibrium dynamics to generate the vectors $\mathbf{r}_i^N$ ($t = 0$) and $\mathbf{v}_i^N$ ($t = 0$) used as an initial conditions in the flow dynamics calculations.

To generate the pressure flow condition, in some studies of molecular dynamics an external force field (F_e) is used, which represents an additional term in the equations of motion and affects all particles in the simulation domain [37,41]. However, in this study it is considered that F_e only affects the particles at the beginning of the simulation region. The F_e enforcement interval is given by $m_1 \leqslant x_1 \leqslant m_2$, where $m_1 = -0.5L_1$ and $m_2 = -0.5L_1 + L_1/Nr$ with Nr equal to 11 and 13 for the cylindrical and rectangular geometries, respectively. Note that the measurement region, i.e., that portion of the geometry in which averages of properties of interest are gathered, is limited to the range $-0.25L_1 \leqslant x_1 \leqslant 0.25L_1$ and therefore it is not affected by the application of the external force field. For both geometries, the magnitude of F_e remained in the range of 0 to $3.3\varepsilon\sigma^{-1}$, with increasing $0.3\varepsilon\sigma^{-1}$, where the maximum value assigned to F_e was the one that develops the flow condition in the cylindrical geometry with $\hat{\beta} = 4$, i.e., without breaking the bonds of the chain molecules.

Once the systems were equilibrated in the absence of external disturbances, the duration of non-equilibrium simulations was two million of integration steps ($\Delta t = 0.001$) for both geometries, of which the first million is used to ensure that the flow reaches the stable state, and the second million is used in the gathering of properties for the averages estimations. To verify that the system reaches the steady state, from the beginning of the simulation

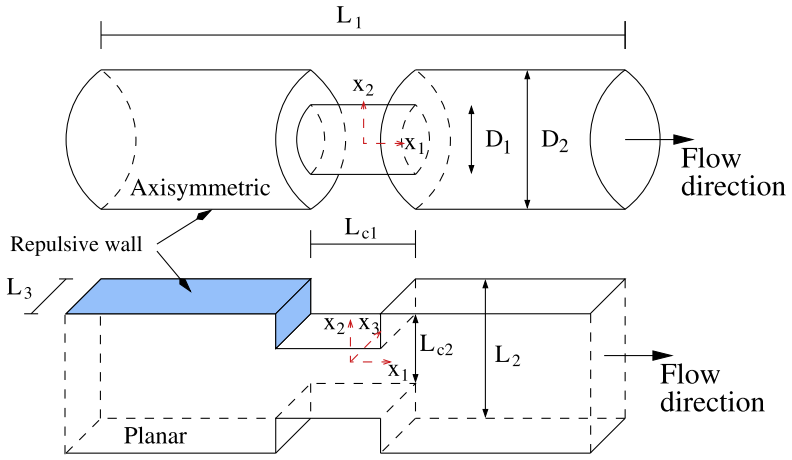

Fig. 2. Schematic representation of cylindrical and rectangular simulation regions.

the velocity profile at the centerline of confinement is monitored, such that in all simulations the stability of the profile was obtained even before the first million of integration steps were reached.

It is noteworthy that for the velocity field that develops in the cylindrical geometry, the type of motion is axisymmetric, where, v_1 and v_2 are different from zero. In the rectangular geometry, the components of the velocity vector v_1 and v_2 are nonzero, so, the type of motion is planar; further, it is important to note that the application of periodic boundary conditions and minimum image in x_3-direction ensures that $v_3 = 0$ with no x_3-dependence.

4. Calculation of molecular properties

4.1. Radius of gyration $\langle R_g^2 \rangle$

Conformations of linear molecules in solution for the two geometries were analyzed. The mean-squared radius of gyration $\langle R_g^2 \rangle$ was obtained by summing the three eigenvalues ($\langle I_1^2 \rangle, \langle I_2^2 \rangle, \langle I_3^2 \rangle$) representing the three main axes of the ellipsoid (containing the segment distribution in the three directions) of the mass distribution tensor **G** [42].

4.2. Stress tensor

In this work, the plane method for non-homogeneous flow [37] is used to calculate the pressure tensor in the fluid, according to the following expression:

$$\sigma_{\varphi\alpha}(\varphi) = \frac{1}{A}\left\langle \sum_{i=1}^{N} \frac{p_{\alpha i} p_{\varphi i}}{m_i} \right\rangle + \frac{1}{2A}\left\langle \sum_{i=1}^{N} F_{\alpha i} \mathrm{sgn}(\varphi_i - \varphi) \right\rangle \quad (4)$$

where $\sigma_{\varphi\alpha}$ is the stress tensor component acting along direction α through a plane normal to the φ axis. A is the area of the plane normal to the φ axis, $\mathrm{sgn}(\varphi_i - \varphi)$ is equal to one if $\mathrm{sgn}(\varphi_i - \varphi) > 0$ and to -1 if $\mathrm{sgn}(\varphi_i - \varphi) < 0$. Furthermore, $F_{\alpha i}$ the α -component of the force acting on particle i, and $p_{\alpha i}$ and $p_{\varphi i}$ are the α and φ components of the momentum of particle i, respectively. The stress tensor $\boldsymbol{\sigma}$ is related to the non-equilibrium components of the pressure tensor such that $\boldsymbol{\sigma} = -\mathbf{P}$. The total stress $\boldsymbol{\sigma}$ implies the contribution of the pressure and that of the viscous stress, such that $\boldsymbol{\sigma} = -p\mathbf{I} + \boldsymbol{\tau}$. In molecular dynamics the total normal stress contains the non-separable contributions from the viscous stress τ and pressure $p\mathbf{I}$. The plane method allows for the calculation the stress components σ_{11} and σ_{22} for planar and axisymmetric geometries. It is important to mention that in recent works using molecular dynamics [43,44], it has been found that normal stress differences depend strongly on the internal energy (kinetic or configurational). Independently of the thermostat used, the results show an underestimate in the value of N_1, which is smaller than that using a kinetic thermostat.

In the flow through a contraction–expansion, the fluid experiences shear stresses at the walls of the geometry. In this regard, previous works with molecular dynamics [45,46] indicated that predictions of shear stresses are different when the thermostat is applied to each molecular site (atomic thermostat) instead of a molecular thermostat applied to the center of mass of the molecules. Travis et al. [45] simulated a simple shear flow of a liquid using a rigid molecular model, where results indicate that the transport properties computed using an atomic thermostat are identical to those obtained with a molecular thermostat at the reduced shear rate of 2.0. Besides the fact that the thermostat is applied to velocity components normal to the flow direction, in this investigation a more flexible model is used and the reduced shear rates achieved in the contraction region were not larger than 0.7.

5. Simple shear flow

In the introduction section, the experiments conducted by Nigen and Walters [1] reveal that the excess pressure drop occurs in axisymmetric but not in planar contraction–expansion geometries, when the viscosity of the fluid non-Newtonian is similar to its Newtonian counterpart. On the other hand, there is experimental evidence that in planar contraction–expansion micro-geometries, the non-Newtonian fluid exhibits a higher-pressure drop than that of the solvent used in the solution, because the viscosity of the non-Newtonian fluid is larger than that of the solvent. Presumably, the difference in viscosities may be responsible for the observed higher-pressure drop.

In this work, the densities of the Boger and L-J fluids are fixed at 0.84 and 0.87, respectively, ensuring that fluids exhibit the same viscosity in the Newtonian low shear rate region of the flow curve (η versus $\dot{\gamma}$). A Boger fluid with concentration per site (ϕ) expressed as site number fraction equal to 0.10 was considered for the pressure drop simulations. Here, the site number fraction is the ratio of the solute number of sites and the total number of sites (solute and solvent). This concentration is the same to that used elsewhere [7,40] and it was selected to ensure a dilute regime according to the value of the critical concentration (c^*). In reduced units, c^* is given by $c^* = 3E_l/4\pi R_g^3$ where R_g is the radius of gyration obtained from equilibrium molecular dynamics (with a value of 2.25). It is worth mentioning that the relaxation time of the Boger fluid is

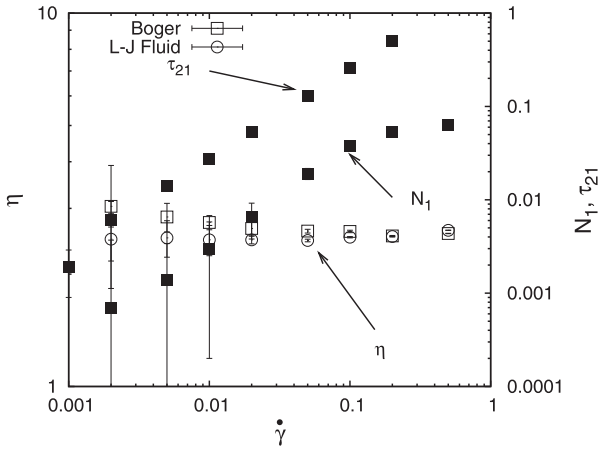

Fig. 3. Reduced shear viscosity (η), shear stress (τ_{21}) and first normal stress difference (N_1) versus shear rate ($\dot{\gamma}$) for the Boger and L-J fluids.

estimated (7.9) from the Rouse expression, $\lambda = 6[\eta]E_l\eta_s/\pi^2\rho T$, where, $[\eta]$ is the intrinsic viscosity and η_s is the solvent viscosity.

Although molecular size and shape obtained from the radius of gyration and its eigenvalues depend on the selected model, the ratio of the eigenvalues $[I_1^2/I_3^2 : I_2^2/I_3^2 : I_3^2/I_3^2]$ is known to be independent of this choice. For polymeric solutions this ratio is [14.8:3.06:1.0], predicted by the "self avoiding random-walk" model [47]. The Boger fluid has an eigenvalue ratio of [15.0:3.09:1.0].

The fluids were subjected to simple shear flow (Couette type) at the same conditions of temperature and density used in the contraction–expansion geometries. Simple shear flow was simulated using the SLLOD method [38], where the temperature was kept constant by coupling the equations of motion to the Nose–Hoover thermostat. Because of this characterization, Fig. 3 shows the variation of the shear viscosity (η) as a function of shear rate ($\dot{\gamma}$) for both fluids. Additionally, the first normal stress difference N_1 and shear stress τ_{21} are also shown for the Boger fluid. N_1 is quadratic at low shear rates, but with a weaker dependence for increasing shear rates. Notice that the Boger fluid possesses low elasticity, since N_1 shows values lower than those of the corresponding shear stress τ_{21}. Fig. 3 exhibits that the viscosity of the L-J fluid is almost constant, around a value of 2.5, in the range of simulated shear rates ($0.002 \leqslant \dot{\gamma} \leqslant 0.5$) and N_1 is zero, which is a good approximation to a Newtonian fluid. The viscosity of the Boger fluid is slightly larger than that of the L-J fluid in the range $0.002 \leqslant \dot{\gamma} \leqslant 0.02$, but past $\dot{\gamma} = 0.02$, the viscosity of both fluids is the same. As mentioned, the reduced density of the solution ($\rho = 0.84$) and L-J fluid ($\rho = 0.87$) was selected to ensure that both fluids exhibit the same shear viscosity, allowing a univocal analysis of the elastic response of the fluids under extensional flow conditions.

6. Results

In this section, we present results of the pressure drop, extensional strain rate and molecular conformations that the fluids exhibit through the geometries already detailed. These variables were chosen on the basis that in previous works [39,30,7], where, it has been shown that the pressure drop is closely related to the extensional viscosity, or the resistance to extensional flow.

Results were obtained for a number of time-averaged fluid properties. To determine an average property, we divide the test region into a sufficient number of slices (for velocity, radius of gyration) or planes (for stress profiles). Then, we calculate the time-averaged property for each slice or plane. For example, we add the x_1-component of the particle velocities in each slice and then we average over the number of particles in that slice at each time step. Finally, the velocity profile is obtained by computing the time average velocity for each slice during the simulation. Similar considerations for the stress profiles are made.

6.1. Prediction of the excess pressure drop (epd)

In this work we use the planes method to estimate the σ_{11} and σ_{22} components, corresponding to the flow and gradient directions, respectively. Elsewhere [40,7] we have already detailed the calculation of the stress components in rectangular geometries, so now we focus on explaining this calculation in the cylindrical geometry. For this sake, a cylinder with a length of $0.5L_1$ and a diameter of $D_p = 1\sigma$ is placed in the measurement region along the centerline of confinement, which is divided into Np_1 (=50) cross sections. Because of these cuts, a $Np_1 - 1$ rings and circles perpendicular to the radial and axial direction are available, respectively. The rings, with D_p diameter are used to estimate the stress tensor component σ_{22}, considering that each one forms a normal plane to the radial coordinate with an area equal to $0.5\pi D_p L_1/(Np_1 - 1)$. According to the planes method, the estimate of σ_{22} involves calculating the force in the radial direction that a particle i experiences when interacting with a particle j, and the line of interaction crosses the plane whose radial coordinate is $r_p = 0.5\sigma$. As already mentioned, the radial force of the particle i is obtained by knowing its angular coordinate and scalar components of the force in the x_2 and x_3 directions. Calculation of the extensional stress σ_{11} involves circular planes normal to flow direction with an area of $0.25\pi D_p^2$.

With the planes method, the profiles of the $\sigma_{11}(x_1)$ and $\sigma_{22}(x_1)$ components of the stress tensor for planar and axisymmetric geometries are estimated, respectively, within the simulation region and in the flow direction. With $\sigma_{22}(x_1)$, pressure profiles $P(x_1)$ are obtained, where each profile corresponds to a given volumetric flow (Q), where Q is obtained by multiplying the average velocity $\langle v \rangle$ by the flow area A_f, both measured at the beginning of the measurement region. The average velocity is the mean value of the velocity evaluated in the central line of confinement ($x_2 = 0$). A_f is equal L_2L_3 and $0.25\pi D_2^2$ in the planar and axisymmetric geometries, respectively.

In a 2:1:2 planar geometry, Castillo-Tejas et al. [7] simulated the flow of L-J and Boger fluids but at a slightly larger density. Results reveal that the pressure drop is the same in both fluids. This equality arises from the pressure variation in the flow direction (x_1), which was similar for a given Q. Now, Fig. 4 shows the pressure as a function of axial coordinate for the axisymmetric geometry with $\hat{\beta} = 2$ and a flow rate of 230; in the inset the planar geometry with the same $\hat{\beta}$ is shown with $Q = 106$. First, in the planar configuration we observe that the pressure profile is similar in both fluids, even though the L-J fluid pressure is slightly larger than in the Boger fluid. Prior the contraction, the pressure has a value of 19 and 16.6 for L-J fluid and Boger fluid, respectively; and the largest loss occurring at the entrance of the contraction ($x_1 = -7.42$). Within the contraction, pressure continues decreasing down to a minimum prior to a recovery at $x_1 = 20.0$. The range of flow rates achieved in the simulations for the planar configuration was $0 \leqslant Q \leqslant 187.0$. The important issue here is that the pressure drop is the same for both fluids.

A very important result is that, in contrast, we observe a higher-pressure drop in the axisymmetric geometry. The pressure at the beginning of the measurement region ($x_1 = -40.0$) is 27.35 and 23.60 for the Boger and L-J fluids, respectively, demonstrating that prior to the entry region the pressure is higher in the Boger fluid, in contrast to the behavior observed in the planar configuration. In both geometries, the highest-pressure loss occurs when the fluid enters the contraction ($x_1 = -7.42$), and when the fluid leaves it,

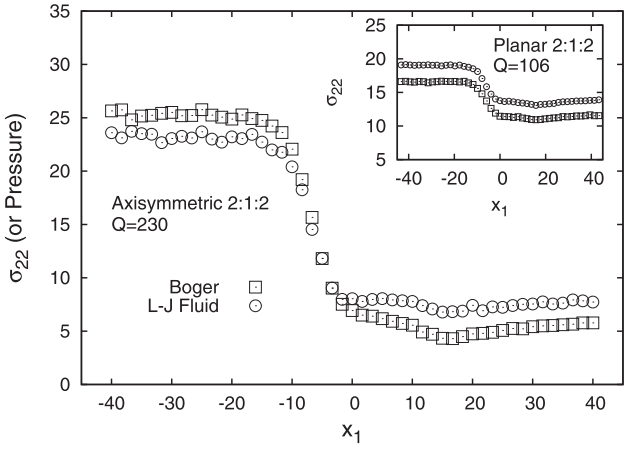

Fig. 4. Variation of the reduced normal stress (σ_{22}) (or pressure) evaluated at the central line of confinement as a function of the axial coordinate (x_1) in the axisymmetric geometry for both fluids. In the inset, the planar geometry results are included.

the pressure is higher in the L-J fluid. In both configurations a repulsive potential was used to simulate the wall effect such that with varying force of attraction to the walls, the fluid may slip at the surfaces [48], reducing the friction between layers of fluid, and therefore, less dissipation leads to a small reduction in the pressure prior to contraction.

The total pressure drop, $\Delta P = P_0 - P_1$ is obtained from pressure the profiles $P(x_1)$, where P_0 and P_1 are the pressures at the beginning and end of the measurement region, corresponding to the planes located at $x_1 = \mp 0.25L_1$. Fig. 5 shows ΔP as a function of flow rate Q for both configurations with $\hat{\beta} = 2$, and in the inset, ΔP is also shown for the cylindrical geometry for $\hat{\beta} = 4$. Although the maximum value of F_e in the simulations was $3.3\varepsilon\sigma^{-1}$, the maximum flow rate reached was 181.0 in the planar 2:1:2 geometry, 268.0 in the 2:1:2 cylindrical geometry and 50.0 in the 4:1:4 axisymmetric geometry, indicating that upon increasing $\hat{\beta}$ the limiting flow rate decreases.

Fig. 5 shows that when the fluids have the same shear viscosity, ΔP is the same for both fluids in the **planar geometry**, which is consistent with the results obtained by Nigen and Walters [1]. Note that the variation of ΔP with Q is linear (with a slope proportional to the viscosity of the system) up to a flow rate of 126.0, and thereafter is non-linear. This slope change reveals the strain hardening of the viscosity under extensional strain, and it is observable in the L-J fluid. Notice that the L-J fluid with constant viscosity may exhibit non-Newtonian behavior that strictly does not correspond to a Newtonian fluid. Non-Newtonian effects in L-J fluids have already been reported previously [49,50].

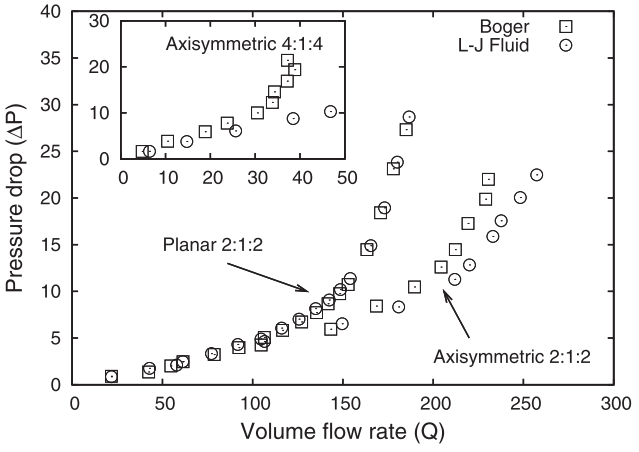

Fig. 5. Reduced pressure drop (ΔP) as a function of the flow rate (Q), for the Boger and L-J fluids in both geometries. In the inset, the 4:1:4 axisymmetric geometry results are shown.

In the **axisymmetric 2:1:2 geometry**, the variation of $\Delta P(Q)$ is linear up to a flow rate of 143.0 and 180.0 in Boger and L-J fluids, respectively, and thereafter, ΔP increases with Q with a steeper slope (0.25). At flow rates lower than 143.0, ΔP is the same in both fluids, and for larger flow rates, ΔP is higher in the Boger fluid than that of the L-J fluid for the same Q, predicting values of the excess in pressure drop (*epd*) larger than one. This excess pressure drop appears at the onset for slope change in the $\Delta P(Q)$ curve. The inset in Fig. 5 shows that upon increasing the contraction ratio ($\hat{\beta}$) the pressure excess in the Boger fluid appears at Q values five times lower than for $\hat{\beta} = 2$, indicating that the reduction in the flow area increases the dissipation under extensional flow. If we assume that the product ΔPQ is proportional to the dissipation, for a given flow rate the 4:1:4 geometry produces higher dissipation.

For a contraction ratio of two, Fig. 5 shows that the total pressure drop in the planar configuration is larger than that in the axisymmetric case; this result is not consistent with experimental measurements [1]. As mentioned in the beginning of this section, the estimation of stress is performed with the method of planes, such that 49 rings perpendicular to the radial direction are considered. Each ring has a diameter of one and is located on the centerline of confinement ($x_2 = 0$). Under Poiseuille flow through a circular conduit for the Boger fluid (at same density, $\rho = 0.84$, used here) we obtained the variation of reduced density (ρ) as a function of radial coordinate (r). Results show that the fluid is ordered in layers at the immediate vicinity of the tube wall, which disappear toward the centerline of confinement. However, in the range $0 \leqslant r \leqslant 0.5$ the density is about 0.65, which is lower than 0.84. Since the rings to measure σ_{22} are located at this portion of the measurement region, perhaps this is the reason by which the total pressure drop in the axisymmetric configuration is smaller than in the planar one. It is noteworthy that this decrease in density when r tends to zero disappears with increasing density of the system, and it is not present in rectangular geometries [48]. We are currently giving attention to these issues to identify the causes of this particular behavior.

In a previous work [7] it was predicted that for a planar geometry, the pressure drop of a Boger fluid and the L-J fluid is similar for a given volume flow rate, provided that both have the same shear viscosity. This equality of pressure drop is related to similar pressure profiles, extensional strain rate and viscous dissipation. To corroborate this, in Fig. 6, the extensional strain rate ($\dot{\varepsilon}$) is plotted as a function of the axial coordinate (x_1) for Boger and L-J fluids in the axisymmetric 4:1:4 ($Q = 38$) and planar 2:1:2 ($Q = 106$) contraction–expansion geometries. The figure shows that in the planar configuration, $\dot{\varepsilon}$ is the same throughout the simulation region for both fluids, which is consistent with pressure drop shown in the Fig. 5 and with previously reported results [7]. In contrast to the planar case, at the contraction entry length $x_1 = -7.42$ (point of maximum pressure drop) of the axisymmetric 4:1:4 geometry, the extensional strain rate is larger in the Boger fluid than in the L-J fluid, which is consistent with the larger ΔP exhibited by the Boger fluid in Fig. 5. Extensional strain rate $\dot{\varepsilon}$ goes through a maximum of 0.52 and 0.72 in the L-J and Boger fluids, respectively, and at the contraction exit length $13.0 \leqslant x_1 \leqslant 20$, both fluids go through a minimum of $\dot{\varepsilon}$ with an approximate value of 0.34. The maximum and minimum in extensional strain rate is associated to the increase and decrease in velocity (v_1) that the fluids exhibit in the contraction; and $\dot{\varepsilon}$ hovers around zero in those portions of the measurement region where the velocity remains constant.

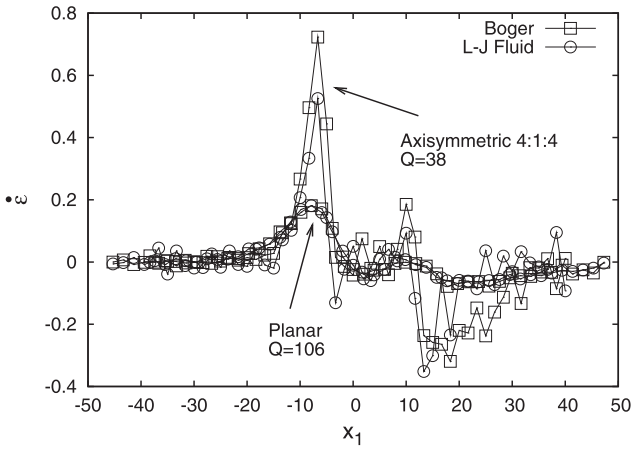

Fig. 6. Variation of reduced extensional strain rate ($\dot{\varepsilon} = \Delta v_1/\Delta x_1$) as a function of the axial coordinate (x_1) in the axisymmetric geometry (4:1:4) for both fluids is compared to predictions in the planar geometry.

In Fig. 5, an excess pressure drop for the Boger fluid in axisymmetric configurations is predicted, but not in the planar geometry. This excess pressure drop is usually presented as the extra pressure drop lost by the reduction in fluid flow area (ΔP_{Entry}), given by:

$$\Delta P_{Entry} = \Delta P - \Delta P_0 - \Delta P_1 \tag{5}$$

where ΔP is the total pressure drop shown in Fig. 5, ΔP_0 and ΔP_1 are the pressure drops at developed flow conditions, before and after contraction. As shown in Fig. 4, the pressure loss before and after the contraction is practically negligible, so that ΔP represents a direct measurement of the pressure loss caused by the reduction in flow area, such that, $\Delta P_{Entry} \sim \Delta P$. Based on the above, the dimensionless pressure drop (ΔP_{Adim}) may be defined as follows:

$$\Delta P_{Adim} = \Delta P_{Entry}(De, Q)/\Delta P_{Entry-LJ}(De = 0, Q) \tag{6}$$

where $\Delta P_{Entry}(De, Q)$ is the pressure drop experienced by the molecules of the Boger fluid at a given volume flow rate, and $\Delta P_{Entry-LJ}(De = 0, Q)$ is the pressure drop experienced by L-J fluid, at the same conditions.

In Fig. 7 we show a remarkable prediction: the excess pressure drop (*epd*) for the three geometries is plotted with Deborah number ($De = \lambda\dot{\gamma}_{App}$), where, λ is the relaxation time and $\dot{\gamma}_{App}$ as the apparent shear rate. The latter is $\langle v_c\rangle/H$, where $\langle v\rangle_c$ is the mean velocity of fluid in contraction and H is $0.5Lc_2$ and $0.5D_1$ for planar

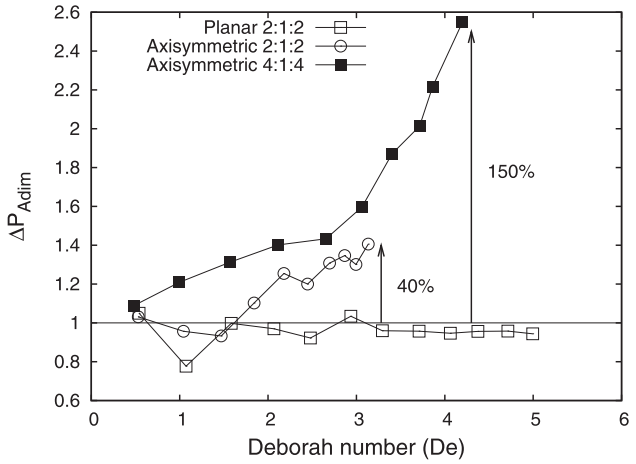

Fig. 7. Dimensionless pressure drop $\Delta P_{Adim} = \Delta P_{Entry}(De, Q)/\Delta P_{Entry-LJ}(De = 0, Q)$ as a function of Deborah number *De* for the Boger fluid in the three geometries.

and axisymmetric configurations, respectively. In the planar geometry, the dimensionless pressure drop ΔP_{Adim} reaches values lower than those of the L-J fluid throughout the range of Deborah numbers, except *De* equal to 0.5 and 3.0. In the 2:1:2 axisymmetric contraction–expansion ΔP_{Adim} decreases below one slightly at $1.0 \leqslant De \leqslant 1.5$ but rises to levels near 40% at $De = 3.13$. More drastic is the rise observed in the 4:1:4 axisymmetric geometry, where, increases over 150% are predicted even for low values of Deborah number.

In a recent paper [51], numerical predictions of the excess pressure drop for the flow of FENE-CR fluids through a 4:1:4 contraction–expansion geometry are exposed. Various forms of this model possessing first normal stress differences weaker than quadratic and high levels of extensional viscosity are able to predict enhanced *epd*, up to values around 28%, which are quite small to those observed experimentally. This value of the *epd* corresponds to a Deborah number of 70, while in the range $0 \leqslant De \leqslant 4$, authors predict an *epd* value lower than 5%. In this investigation and for a $De = 3.2$, a value in *epd* of 40% and 60% for planar and axisymmetric configurations are predicted, respectively. Experimentally, Rothstein and McKinley [3] reported an increase of approximately 60% at a Deborah number of 3.2 in the flow of a Boger fluid through a 4:1:4 axisymmetric configuration.

To assess the inertial effects, the maximum Reynolds number achieved in the simulations was 11.3 and 6.6 for 2:1:2 planar and axisymmetric configurations, respectively. With $\hat{\beta} = 4.0$, a Reynolds number of 2.21 in the axisymmetric configuration was reached. As shown in Fig. 3 for the Boger fluid, the first normal stress difference N_1 exhibits a weaker-than-quadratic dependence for increasing shear rates, and therefore, Boger fluid possesses low elasticity; and hence, moderate to low Reynolds numbers are achieved in the simulations. It is important to mention that inertial or elastic effects on pressure drop depend on type of contraction–expansion configuration. Perera and Walters [52] found that the pressure drop is five orders larger upon increasing inertia (in terms of the Reynolds number) than that attained with increasing elasticity.

Finally, experimental studies have reported vortex formation at the exit of the contraction with Reynolds numbers of 0.1, whose evolution is qualitatively different in the axisymmetric or planar configurations [2,8]. In this work, simulations were not intended to identify the vortex formation; however, in a previous study of molecular dynamics [6], we have predicted vortices at the outlet of a 4:1:4 planar contraction–expansion.

6.2. Boger fluid: a comparative between 2:1:2 planar and axisymmetric geometries

It is apparent that the fluid response to extensional strain for a given volume flow rate is responsible for the observed pressure drop. It is now important to analyze the cause of different responses exhibited by the Boger fluid in 2:1:2 axisymmetric and planar geometries. According with the results shown in Fig. 7, we choose a $De \sim 3.0$ and $Re \sim 6.6$ to analyze the molecular configuration and extensional strain rate of the Boger fluid in both geometries, taking care that the inertial and elastic effects are similar in the comparisons. First, respect to the final configuration, Fig. 8a shows the side view of the molecular conformations of the Boger fluid, corresponding to the axisymmetric contraction–expansion. When the molecules enter the contraction, they experience an elongation in the direction of flow, and at the contraction exit, they have a more coiled conformation than that prior to the contraction. As in the planar configuration (not shown), the molecules undergo extensional flow when they enter the axisymmetric contraction, and there are almost no differences in molecular conformation in regions distant from the contraction. In the axisymmetric case,

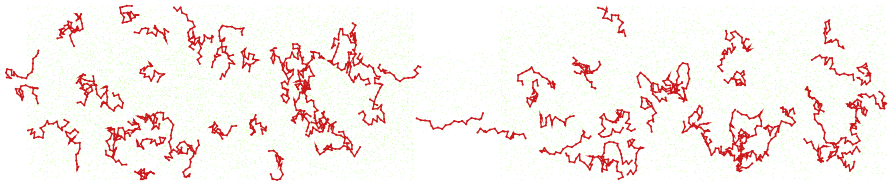

(a) Axisymmetric 2:1:2, lateral view

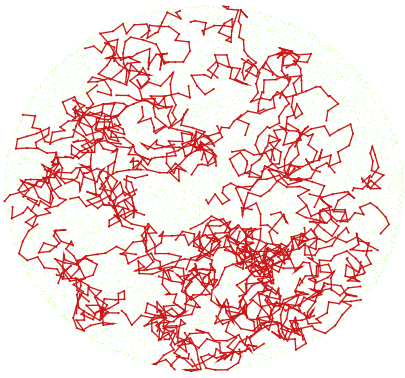

(b) Axisymmetric 2:1:2, transversal view

Fig. 8. (a) Lateral and, (b) transversal view of the position vector $\mathbf{r}_i^N(t)$ for the Boger fluid in the 2:1:2 geometry.

the molecules fill the whole domain of simulation in the gradient direction (x_2) (see Fig. 8b).

It is likely that differences in extensional strain rate exhibited by Boger fluid in both configurations are related to conformation of their molecules. Fig. 9 presents the variation of mean-square mass distribution tensor eigenvalue $\langle I_2^2\rangle$ of molecules in the Boger fluid as a function of the axial coordinate x_1, in both geometries at the same Deborah number. The magnitude of the eigenvalue defines the distribution of molecule monomers in the gradient direction x_2. The first interesting observation is that at the beginning and end of the measurement region, the size of the molecule in the gradient direction is the same in both configurations, with an approximate value from 0.24 to 0.26. To enter the contraction, the molecules experience a compression in the gradient direction, which is manifested by a minimum in $\langle I_2^2\rangle$. This corresponds to a minimum value of 0.19 and 0.11 in planar and axisymmetric configurations, respectively. The important result is that a larger change in molecular conformation is then observed in the axisymmetric geometry.

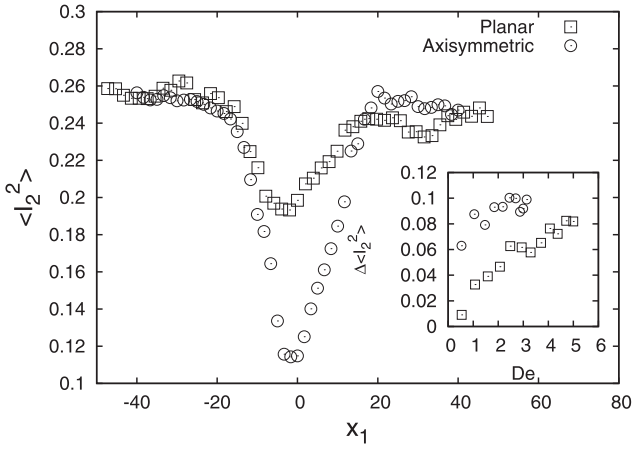

Fig. 9. Variation of mean-square mass distribution tensor eigenvalue $\langle I_2^2\rangle$ as a function of the axial coordinate x_1 for the Boger fluid in the 2:1:2 geometry and $e = 3.0$. In the inset, the conformational change $\Delta\langle I_2^2\rangle$ with *De* is included.

The variation in the molecular conformation in both geometries reflects the larger pressure drop predicted in the axisymmetric geometry. In the inset of Fig. 9, the variation of $\Delta\langle I_2^2\rangle$ is presented as a function of the Deborah number for both geometries, where $\Delta\langle I_2^2\rangle = \langle I_2^2\rangle_0 - \langle I_2^2\rangle_c$ is the difference between the mean-square mass distribution eigenvalue evaluated at the beginning of the measurement region ($\langle I_2^2\rangle_0$) and that evaluated at the entrance of the contraction ($\langle I_2^2\rangle_c$). In the inset is shown that $\Delta\langle I_2^2\rangle$ is positive, increasing almost linearly with the Deborah number in both geometries. The average of $\Delta\langle I_2^2\rangle$ reveals a value of 80% higher in the axisymmetric case respect to the planar geometry.

The magnitude of the change in molecular conformation along the flow trajectory is then the important factor. Rothstein and McKinley [3,8] mentioned that the pressure drop in the axisymmetric case is associated with the stress-conformation hysteresis cycles whose areas represent the work required to deform the molecule. In Fig. 10, a stress-conformation hysteresis cycle for molecules of solution in two configurations is predicted. The cycle is expressed in terms of first normal stress difference N_1 and the mean-squared radius of gyration R_g^2. At a Deborah number of 3, the total pressure drop is 5.5 and 19.9 for planar and axisymmetric configurations, respectively, such that, the largest area enclosed in the hysteresis loop corresponding to that configuration with the highest pressure drop predicted. Results shown in Fig. 10 indicate the work required to deform the molecules, and that this state of strain is responsible for the dissipation or pressure drop.

Fig. 11 show the variation of the extensional strain rate $\dot{\varepsilon}$ and velocity v_1 (see inset) as functions of the axial coordinate in both geometries for the Boger fluid. The velocity v_1 is larger in the axisymmetric case than in the planar geometry along the entire flow domain. The strain rate goes through a maximum with larger magnitude in the axisymmetric case ($\dot{\varepsilon} = 0.57$) than in the planar geometry ($\dot{\varepsilon} = 0.19$). The peak in the strain rate coincides with the minimum in the mean-square mass distribution tensor eigenvalue I_2^2 observed in Fig. 9. The extensional flow causes the change in molecular conformation that is reflected in the larger pressure

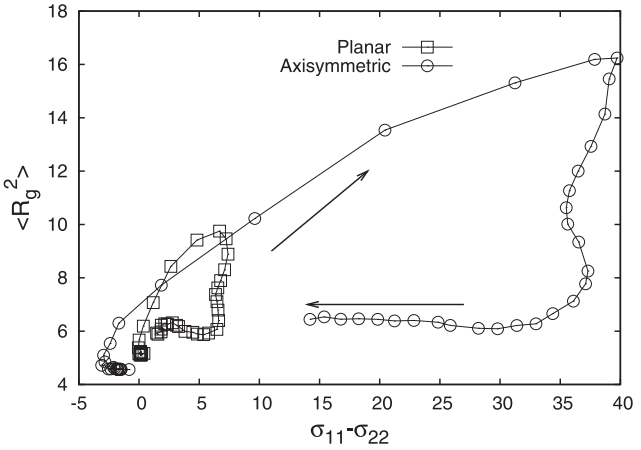

Fig. 10. Mean-square radius of gyration $\langle R_g^2 \rangle$ as a function of normal stress difference $\sigma_{11} - \sigma_{22}$, at Deborah number of 3.0.

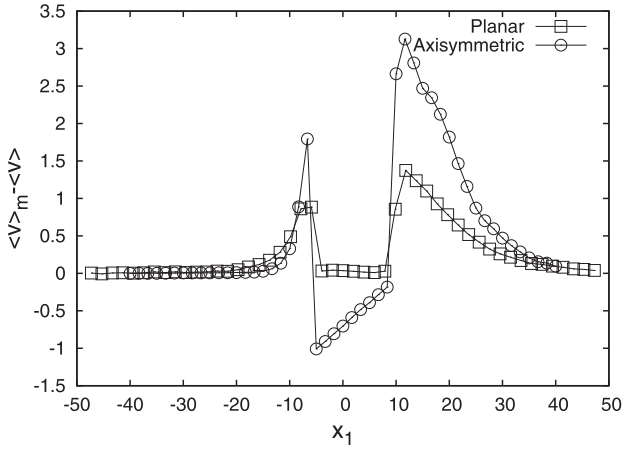

Fig. 12. Variation of the difference of velocities $\langle v \rangle_m - \langle v \rangle$ as a function of the axial coordinate x_1 for the Boger fluid in both geometries with 2:1:2 contraction ratio at $De \sim 3.0$.

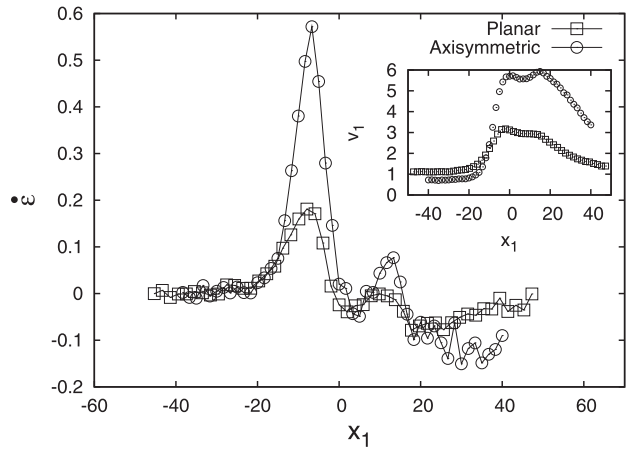

Fig. 11. Variation of reduced extensional strain rate $\dot{\varepsilon}$ for the Boger fluid as a function of the axial coordinate x_1 in both geometries with 2:1:2 contraction ratio at $De \sim 3.0$. In the inset, the velocity field under same conditions is included.

drop predicted in the axisymmetric case for the Boger fluid with respect to the L-J fluid.

7. Discussion and concluding remarks

In this work, molecular dynamics simulations are carried out to describe the rheological behavior of Boger and Lennard-Jones fluids through axisymmetric and planar contraction–expansion geometries, where, both fluids exhibit the same shear viscosity. To produce the flow, an external force term is included to represent the pressure gradient in the equations of motion, which are coupled to Nose–Hoover dynamics to keep the constant temperature in the simulations. The boundaries in gradient direction in the planar and axisymmetric geometries are simulated with a repulsive potential.

Results predict larger pressure drop ΔP in the Boger fluid than that in the L-J fluid in the axisymmetric geometry, while in the planar case, the pressure drop that both fluids exhibit reaches same values. In the axisymmetric geometry the excess pressure drop (ratio of the pressure drop of the Boger fluid to that of the L-J fluid) reaches values larger than 1 when a change in the slope in the $\Delta P(Q)$ curve from linear to non-linear is apparent. The upward change of the pressure profiles is thereby related to the strain hardening of the resistance to extensional deformation (extensional viscosity).

The excess pressure drop (*epd*) depends on the changes in conformation of the molecules, and hence on the elasticity of the molecule, and how the onset of elastic effects are induced or delayed by the specific geometry. Fig. 12 shows the difference in velocities $\langle v \rangle_m - \langle v \rangle$ (where $\langle v \rangle_m$ is the mean velocity of the monomers of molecules and $\langle v \rangle$ is mean velocity of fluid) for the Boger fluid as a function of axial coordinate x_1 in both geometries. Larson [53] has pointed out that this difference in velocities (which is a kind of non-affine motion) is a measure of additional drag forces (hydrodynamic interactions) between the molecules and the solvent in dilute solutions. In the axisymmetric and planar cases, $\langle v \rangle_m - \langle v \rangle$ is zero in regions far from the contraction since the velocity of the chains and that of the solution is the same, and hence, hydrodynamic interactions do not affect the molecular conformation. However, in both configurations, $\langle v \rangle_m - \langle v \rangle$ is larger than zero at input and exit of the contraction, indicating the presence of additional drag forces caused by the non-affine motion through hydrodynamic interactions with the solvent. In the planar case, $\langle v \rangle_m - \langle v \rangle$ is 0.88 and 1.37 at the entry and exit of the contraction, respectively, which contrasts with values of 1.8 and 3.12 of the axisymmetric geometry. Furthermore, in the axisymmetric case, as soon as the fluid enters the contraction $\langle v \rangle_m - \langle v \rangle$ is negative, revealing differences in the motion of the molecules with respect to that of the solution. This non-affine motion is presumably responsible for the increased extension in the molecular conformation. In the planar contraction–expansion, non-affine motion is reduced with respect to the axisymmetric case, where there is a larger change in molecular conformation. The work necessary to deform the molecules causes larger dissipation and hence larger pressure losses in the axisymmetric contraction–expansion geometry.

Finally, a remarkable prediction of the present work is the large increases in *epd* in the 4:1:4 contraction–expansion geometry, even with low values of N_1. The predicted values amount to more than 150%, which are right steps in the direction of predicting the large *epd* levels found experimentally for Boger fluids.

Acknowledgments

The authors are grateful for the financial support from SEP-CONACYT and PROMEP through the projects CB-2008/100195 and PROMEP/103.5/12/2116, respectively.

References

[1] S. Nigen, K. Walters, Viscoelastic contraction flows: comparison of axisymmetric and planar configurations, J. Non-Newtonian Fluid Mech. 102 (2002) 343–359.
[2] K. Walters, M.F. Webster, The distinctive CFD challenge of computational rheology, Int. J. Numer. Methods Fluids 43 (2003) 577–596.
[3] J.P. Rothstein, G.H. McKinley, Extensional flow of a polystyrene Boger fluid through a 4:1:4 axisymmetric contraction/expansion, J. Non-Newtonian Fluid Mech. 86 (1999) 61–88.
[4] P.S. Doyle, E.S.G. Shaqfeh, G.H. McKinley, S.H. Spiegelberg, Relaxation of dilute polymer solutions following extensional flow, J. Non-Newtonian Fluid Mech. 68 (1997) 61–83.
[5] G. Lielins, P. Halin, I. Jaumain, R. Keunings, V. Legat, New closure approximations for the kinetic theory of finitely extensible dumbbells, J. Non-Newtonian Fluid Mech. 76 (1998) 249–279.
[6] J. Castillo-Tejas, A. Rojas-Morales, F. López-Medina, J.F.J. Alvarado, G. Luna-Bárcenas, F. Bautista, O. Manero, Flow of linear molecules through a 4:1:4 contraction–expansion using non-equilibrium molecular dynamics: extensional rheology and pressure drop, J. Non-Newtonian Fluid Mech. 161 (2009) 48–59.
[7] J. Castillo-Tejas, S. Carro, O. Manero, Elastic response from pressure drop measurements through contraction–expansion geometries by molecular dynamics: structural effects in melts and molecular origin of excess pressure drop, Rheol. Acta 52 (2013) 767–783.
[8] J.P. Rothstein, G.H. McKinley, The axisymmetric contraction–expansion: the role of extensional rheology on vortex growth dynamics and the enhanced pressure drop, J. Non-Newtonian Fluid Mech. 98 (2001) 33–63.
[9] J.P. Rothstein, G.H. McKinley, Inhomogeneous transient uniaxial extensional rheometry, J. Rheol. 46 (2002) 1419–1443.
[10] S.J. Haward, Z. Li, D. Lighter, B. Thomas, J.A. Odell, X.-F. Yuan, Flow of dilute to semidilute polystyrene solutions through a benchmark 8:1 planar micro-contraction, J. Non-Newtonian Fluid Mech. 165 (2010) 1654–1669.
[11] L. Genieser, R.A. Brown, R.C. Armstrong, Comparison of measured center-plane stress and velocity fields with predictions of viscoelastic constitutive models, J. Rheol. 47 (2003) 1331–1350.
[12] S.J. Haward, J.A. Odell, Z. Li, X.-F. Yuan, Extensional rheology of dilute polymer solutions in oscillatory cross-slot flow: the transient behavior of birefringent strands, Rheol. Acta 49 (2010) 633–645.
[13] S.J. Haward, J.A. Odell, Z. Li, X.-F. Yuan, The rheology of polymer solution elastic strands in extensional flow, Rheol. Acta 49 (2010) 781–788.
[14] S.J. Haward, M.S.N. Oliveira, M.A. Alves, G.H. McKinley, Optimized cross-slot flow geometry for microfluidic extensional rheometry, Phys. Rev. Lett. 109 (2012) 128301.
[15] S.J. Haward, T.J. Ober, M.S.N. Oliveira, M.A. Alves, G.H. McKinley, Extensional rheology and elastic instabilities of a wormlike micellar solution in a microfluidic cross-slot device, Soft Matter 8 (2012) 536–555.
[16] L.E. Rodd, J.J. Cooper-White, D.V. Boger, G.H. McKinley, The inertio-elastic planar entry flow of low-viscosity elastic fluids in micro-fabricated geometries, J. Non-Newtonian Fluid Mech. 129 (2005) 1–22.
[17] L.E. Rodd, J.J. Cooper-White, D.V. Boger, G.H. McKinley, Role of the elasticity number in the entry flow of diluted polymer solutions in micro-fabricated contraction geometries, J. Non-Newtonian Fluid Mech. 143 (2007) 170–191.
[18] Z. Li, X.-F. Yuan, S.J. Haward, J.A. Odell, S. Yeates, Non-linear dynamics of semi-dilute polydisperse polymer solutions in microfluidics: a study of a benchmark flow problem, J. Non-Newtonian Fluid Mech. 166 (2011) 951–963.
[19] Z. Li, X.-F. Yuan, S.J. Haward, J.A. Odell, S. Yeates, Non-linear dynamics of semi-dilute polydisperse polymer solutions in microfluidics: effects of flow geometry, Rheol. Acta 50 (2011) 277–290.
[20] A. Lanzaro, X.-F. Yuan, Effects of contraction ratio on non-linear dynamics of semi-dilute, highly polydisperse PAAm solutions in microfluidics, J. Non-Newtonian Fluid Mech. 166 (2011) 1064–1075.
[21] L. Campo-Deaño, F. Galindo-Rosales, F.T. Pinho, M.A. Alves, M.S.N. Oliveira, Flow of low viscosity Boger fluids through a microfluidic hyperbolic contraction, J. Non-Newtonian Fluid Mech. 166 (2011) 1286–1296.
[22] F.J. Galindo-Rosales, L. Campo-Deaño, F.T. Pinho, E. van Bokhorst, P.J. Hamersma, M.S.N. Oliveira, M.A. Alves, Microfluidic system for the analysis of viscoelastic fluid flow phenomena in porous media, Microfluid Nanofluid 12 (2012) 485–498.
[23] P. Szabo, J.M. Rallison, E.J. Hinch, Start-up of flow of a FENE-fluid through a 4:1:4 constriction in a tube, J. Non-Newtonian Fluid Mech. 72 (1997) 73–86.
[24] P. Wapperom, R. Keunings, Numerical simulation of branched polymer melts in transient complex flow using Pom-Pom models, J. Non-Newtonian Fluid Mech. 97 (2001) 267–281.
[25] M. Aboubacar, H. Matallah, H.R. Tamaddon-Jahromi, M.F. Webster, Numerical prediction of extensional flows in contraction geometries: hybrid finite volume/element method, J. Non-Newtonian Fluid Mech. 104 (2002) 125–164.
[26] M.A. Alves, P.J. Oliveira, F.T. Pinho, Benchmark solutions for the flow of Oldroyd-B and PTT fluids in planar contractions, J. Non-Newtonian Fluid Mech. 110 (2003) 45–75.
[27] D.M. Binding, P.M. Phillips, T.N. Phillips, Contraction/expansion flows: the pressure-drop and related issues, J. Non-Newtonian Fluid Mech. 137 (2006) 31–38.
[28] J.P. Aguayo, H.R. Tamaddon-Jahromi, M.F. Webster, Excess pressure-drop estimation in contraction and expansion flows for constant shear-viscosity, extension strain-hardening fluids, J. Non-Newtonian Fluid Mech. 153 (2008) 157–176.
[29] K. Walters, M.F. Webster, H.R. Tamaddon-Jahromi, The numerical simulation of some contraction flow of a highly elastic liquids and their impact on the relevance of the Couette correction in extensional rheology, Chem. Eng. Sci. 64 (2009) 4632–4639.
[30] H.R. Tamaddon-Jahromi, M.F. Webster, P.R. Williams, Excess pressure drop and drag calculations for strain-hardening fluids with mild shear thinning: contraction and falling spheres problems, J. Non-Newtonian Fluid Mech. 166 (2011) 939–950.
[31] D.M. Binding, K. Walters, On the use of flow through a contraction in estimating the extensional viscosity of mobile polymer solutions, J. Non-Newtonian Fluid Mech. 30 (1988) 233–250.
[32] D.M. Binding, An approximate analysis for contraction and converging flows, J. Non-Newtonian Fluid Mech. 27 (1988) 173–189.
[33] D.M. Binding, Further considerations of axisymmetric contraction flows, J. Non-Newtonian Fluid Mech. 41 (1991) 27–42.
[34] A.S. Lubansky, D.V. Boger, C. Servais, A.S. Burbidge, J.J. Cooper-White, An approximate solution to flow through a contraction for high Trouton ratio fluids, J. Non-Newtonian Fluid Mech. 144 (2007) 87–97.
[35] K. Kremer, G. Grest, Dynamics of entangled linear polymer melts: a molecular-dynamics simulation, J. Chem. Phys. 92 (1990) 5057–5086.
[36] H.R. Warner Jr., Kinetic theory and rheology of dilute suspensions of finitely extensible dumbbells, Ind. Eng. Chem. Fundam. 11 (1972) 379–387.
[37] B.D. Todd, D.J. Evans, P.J. Daivis, Pressure tensor for inhomogeneous fluids, Phys. Rev. E 52 (1995) 1627–1638.
[38] D. Evans, G. Morriss, Statistical Mechanics of Non-equilibrium Liquids, Academic Press, New York, 1990.
[39] S. Nose, A unified formulation of the constant temperature molecular dynamics methods, J. Chem. Phys. 81 (1984) 511–519.
[40] G. González-González, J. Castillo-Tejas, J.P. Aguayo-Vallejo, J.F.J. Alvarado, O. Manero, Predictions of the excess pressure drop of Boger fluids through a 2:1:2 contraction–expansion geometry using non-equilibrium molecular dynamics, Rheol. Acta 48 (2009) 1017–1030.
[41] Z. Zhang, J.S. Hansen, B.D. Todd, Structural and dynamical properties for confined polymers undergoing planar Poiseuille flow, J. Chem. Phys. 126 (2007) 144907.
[42] D.C. Rapaport, The Art of Molecular Dynamics Simulation, Cambridge University Press, United Kingdom, 2004.
[43] P.J. Daivis, B.A. Dalton, T. Morishita, Effect of kinetic and configurational thermostats on calculations of the first normal stress coefficient in non-equilibrium molecular dynamics simulations, Phys. Rev. E 86 (2012) 056707.
[44] W.G. Hoover, C.G. Hoover, J. Petravic, Simulation of two and three dimensional dense fluid shear flows via non-equilibrium molecular dynamics: comparison of time and space averaged stresses from homogeneous Doll's and SIlod shear algorithms with those from boundary driven shear, Phys. Rev. E 78 (2008) 046701.
[45] K.P. Travis, P. Daivis, D.J. Evans, Thermostats for molecular fluids undergoing shear flow: application to liquid chlorine, J. Chem. Phys. 103 (1995) 10638–10651.
[46] K.P. Travis, D.J. Evans, On the rheology of n-eicosane, Molec. Simul. 17 (1996) 157–164.
[47] J. Mazur, C.M. Guttman, F.L. McCracking, Monte Carlo studies of self-interacting polymer chains with excluded volume. II. Shape of a chain, Macromolecules 6 (1973) 872–874.
[48] J. Castillo-Tejas, J.F.J. Alvarado, G. González-Alatorre, G. Luna-Barcenas, I.C. Sanchez, R. Macias-Salinas, O. Manero, Non-equilibrium molecular dynamics of the rheological and structural properties of linear and branched molecules. Simple shear and Poiseuille flows; instabilities and slip, J. Chem. Phys. 123 (2005) 054907.
[49] J. Delhommelle, J. Petravic, D.J. Evans, Reexamination of string phase and shear thickening in simple fluids, Phys. Rev. E 68 (2003) 031201.
[50] J. Delhommelle, J. Petravic, D.J. Evans, Non-Newtonian behavior in simple fluids, J. Chem. Phys. 120 (2004) 6117–6213.
[51] H.R. Tamaddon-Jahromi, M.F. Webster, K. Walters, Predicting numerically the large increases in extra pressure drop when Boger fluids flow through axisymmetric contractions, Nat. Sci. 2 (2010) 1–11.
[52] M.G.N. Perera, K. Walters, Long-range memory effects in flows involving abrupt changes in geometry. Part 2. The expansion/contraction/expansion problem, J. Non-Newtonian Fluid Mech. 2 (1977) 191–204.
[53] R.G. Larson, The Structure and Rheology of Complex Fluids, Oxford University Press, New York, 1999.